Available online at www.sciencedirect.com
ScienceDirect
Journal of Sound and Vibration 312 (2008) 210–233
JOURNAL OF SOUND AND VIBRATION
www.elsevier.com/locate/jsvi

Optimal actuator and sensor placement in flexible structures using closed-loop criteria

Murat Güney, Eşref Eşkinat*

Department of Mechanical Engineering, Boğaziçi University, Bebek, Istanbul 34342, Turkey

Received 17 November 2006; received in revised form 20 October 2007; accepted 22 October 2007
Available online 21 December 2007

Abstract

A closed-loop optimal location selection method for actuators and sensors in flexible structures is developed. The introduced technique simultaneously designs a computationally simple $\mathscr{H}_\infty$ controller and optimizes the location with a gradient-based unconstrained minimization. The $\mathscr{H}_\infty$ controller is a modified version of a normalized coprime controller and obtained by solving control and filter algrebraic Riccati equations (CARE and FARE) approximately. Different types of weights (disturbance input, performance output, sensor noise inputs, etc.) are incorporated to the generalized plant. Hence, the approximate ARE solutions take into consideration the signal weightings in the system. Since an iterative gradient search algorithm is used, the partial derivatives of the approximate AREs with respect to the design parameters are taken. Developed method is detailed and illustrated by a Euler–Bernoulli beam example.

1. Introduction

Vibration suppression in flexible structures such as beams, plates, space shuttles, large antennas, etc. is a common engineering problem. Exposed to external disturbances, a flexible structure deforms. These deformations need to be eliminated or reduced to a certain level by means of control forces applied by the actuators. The control forces are determined by a controller using the feedback of the deformations obtained by the sensors. Most often, the number of actuators and sensors are limited. Therefore, one has to find the best actuator and sensor locations to achieve the maximum possible vibration suppression. This problem is called the best (optimal) location selection of actuators and sensors.

To mention a few of the different I/O selection methods [1], one can use a naive and simple approach for I/O selection that accepts configurations, which are both state controllable and state observable. These qualitative properties of a system can be checked in various ways such as controllability/observability Gramians, matrices, etc. [2,3]. In literature there are rare optimal selection methods based on this simple idea. The quantitative measures of controllability and observability are preferred since they can give enough information for comparing the different combinations of actuator and sensor locations.

*Corresponding author.
E-mail addresses: muratgun@boun.edu.tr (M. Güney), eskinat@boun.edu.tr (E. Eşkinat).

0022-460X/$ - see front matter © 2007 Elsevier Ltd. All rights reserved.
doi:10.1016/j.jsv.2007.10.051

Among the techniques, which are used for checking controllability and observability, Gramians can serve as an more rigorous quantitative measure. For optimal actuator and sensor locations, Georges [4] defines transient controllability and observability Gramians at a time T and uses a function of them as an energy-based optimization metric. Hać and Liu [5] has dealt with optimal placement of actuators and sensors of flexible structures which are exposed to external transient and persistent disturbances. They develop a certain criterion which contains some measure of controllability and observability Gramians. Another study about optimal actuator and sensor location selection, which uses controllability and observability Gramians, is the paper of Gawronski and Lim [6]. They derive some structural properties of flexible structures in modal and balanced coordinates where the controllability and observability Gramians are equal. The diagonal entries of Gramians are Hankel singular values, which give a measure for controllability and observability.

Maghami and Joshi [7] develop an optimal actuator and sensor location selection technique for large-order flexible space structure, where the placement of actuators and sensors is optimized in order to move the zeros in right-half-plane to the left-half-plane.

Another group of I/O selection methods use different measures of singular value decompositions (SVD) of a configuration such as the minimum singular value, the maximum singular value, the condition number, the relative gain array. Morari [8] suggests to chose combinations with large minimum singular value ($\underline{\sigma}(P)$) to improve the tracking following and disturbance rejection properties of a plant.

Arabyan et al. [9] deal with the physical plant. They obtain an expression for the residual deformation of the system and the maximum singular value of this expression needs to be kept small according to their best location selection criteria. The actuator and sensor location with the smallest residual deformation is the best place for the point actuators.

The robust coprime controller design Hiramoto et al. [10] has developed is a modified version of the robust stabilization of coprime factors [2,11].

With the exception of Ref. [10], none of the methods mentioned above use closed-loop criteria to select the location of actuators and sensors. Signal weights, which are an integral part of controller design, are also not considered.

Our study introduces a closed-loop actuator/sensor selection technique, which includes a coprime controller design. The optimization metric to be minimized is the $\mathscr{H}_2$-norm of the closed-loop plant including the signal weights.

Our study introduces a closed-loop actuator/sensor selection technique, which includes a coprime controller design. The optimization metric to be minimized is the $\mathscr{H}_2$-norm of the closed-loop plant including the signal weights.

The designed controller is an improved version of the coprime controller developed Hiramoto et al. [10]. Their controller was designed for the physical plant without signal weightings and assumed zero damping. However, in our study the modal damping is preserved and the physical plant is augmented with signal weightings. By putting the generalized plant (with signal weightings) into more convenient modal state space form, approximate but simple solutions of the generalized algebraic Riccati equations (AREs), and hence simple $\mathscr{H}_\infty$ controllers are obtained.

The point actuators and the rate sensors are assumed to be collocated. That is, the rate sensors are installed at the same locations with the actuators.

In the optimization part, a simple gradient-based algorithm is used to obtain the optimum locations. An simply supported Euler–Bernoulli beam example is given to illustrate the developed approach.

2. Model of the structure

The equation of motion of the flexible structure with collocated point actuators and sensors can be given in nodal form as

$$\mathbf{M}\ddot{\mathbf{q}} + \mathbf{C}\dot{\mathbf{q}} + \mathbf{K}\mathbf{q} = \mathbf{L}_\mathbf{w}\mathbf{d} + \mathbf{L}_\mathbf{u}\mathbf{u},$$

$$\mathbf{z} = \mathbf{C}_{\mathbf{zq}}\mathbf{q} + \mathbf{C}_{\mathbf{zv}}\dot{\mathbf{q}},$$

$$\mathbf{y} = \mathbf{C}_{\mathbf{yq}}\mathbf{q} + \mathbf{C}_{\mathbf{yv}}\dot{\mathbf{q}}, \tag{1}$$

where $\mathbf{q}$ is the vector of displacements, $\mathbf{w}$ and $\mathbf{u}$ are the vectors of disturbances and control inputs acting on the nodes, respectively. $\mathbf{y}$ is $N_y \times 1$ the output vector. The matrix $\mathbf{L_u}$ of dimensions $N \times N_u$, is a function of the point actuators. N and N_u denote the degree of freedom of the structure and the number of point actuators, respectively.

$\mathbf{C_{yq}}$ is the $N_r \times N$ measured output displacement matrix, and $\mathbf{C_{yv}}$ is the $N_r \times N$ measured output velocity matrix.

$\mathbf{z}$ is the performance output vector of dimensions $N_z \times 1$, where $\mathbf{C_{zq}}$ and $\mathbf{C_{zv}}$ are performance output displacement and performance output velocity matrices, respectively.

If only rate sensors are installed and are collocated with actuators, no displacement is measured, $\mathbf{C_{yq}} = 0$, and $\mathbf{C_{yv}}$ becomes

$$\mathbf{C_{yv}} = \mathbf{L}_u^{\mathrm{T}}.$$

Assuming proportional damping and following the procedure in Ref. [12], Eq. (1) can be transformed to the equation of motion in the modal coordinates aso

$$\begin{aligned} \ddot{\mathbf{q}}_\mathbf{m} + 2\mathbf{Z}\boldsymbol{\Omega}\dot{\mathbf{q}}_\mathbf{m} + \boldsymbol{\Omega}^2\mathbf{q}_\mathbf{m} &= \mathbf{L}_{\mathbf{w,m}}\mathbf{d} + \mathbf{L}_{\mathbf{u,m}}\mathbf{u}, \\ \mathbf{z} &= \mathbf{C}_{\mathbf{zq,m}}\mathbf{q}_\mathbf{m} + \mathbf{C}_{\mathbf{zv,m}}\dot{\mathbf{q}}_\mathbf{m}, \\ \mathbf{y} &= \mathbf{C}_{\mathbf{yv,m}}\dot{\mathbf{q}}_\mathbf{m}. \end{aligned} \tag{2}$$

In Eqs. (2), the newly defined variables are $\mathbf{q} \equiv \boldsymbol{\Phi}\mathbf{q}_m$, $\mathbf{L_{w,m}} \equiv \boldsymbol{\Phi}^{\mathrm{T}}\mathbf{L_w}$, $\mathbf{L_{u,m}} \equiv \boldsymbol{\Phi}^{\mathrm{T}}\mathbf{L_u}$, $\mathbf{C_{zv,m}} \equiv \mathbf{C_{zv}}\boldsymbol{\Phi}$, $\mathbf{C_{zq,m}} \equiv \mathbf{C_{zq}}\boldsymbol{\Phi}$, $\mathbf{C_{yv,m}} \equiv \mathbf{C_{yv}}\boldsymbol{\Phi}$, $\boldsymbol{\Omega} \equiv \mathrm{diag}\{\omega_1, \omega_2, \ldots \omega_N\}$ and $\mathbf{Z} \equiv \mathrm{diag}\{\zeta_1, \zeta_2, \ldots \zeta_N\}$, where $\boldsymbol{\Phi}$ is the mode shape matrix.

The state space realization of Eqs. (2) is

$$\begin{aligned} \dot{\hat{\mathbf{x}}} &= \hat{\mathbf{A}}\hat{\mathbf{x}} + \hat{\mathbf{B}}_1\mathbf{d} + \hat{\mathbf{B}}_2\mathbf{u}, \\ \mathbf{z} &= \hat{\mathbf{C}}_1\hat{\mathbf{x}}, \\ \mathbf{y} &= \hat{\mathbf{C}}_2\hat{\mathbf{x}}, \end{aligned} \tag{3}$$

where $\hat{\mathbf{x}} = [\mathbf{q}_\mathbf{m}^{\mathrm{T}},\ \dot{\mathbf{q}}_\mathbf{m}^{\mathrm{T}}]^{\mathrm{T}}$ and,

$$\hat{\mathbf{A}} = \begin{bmatrix} \mathbf{0} & \mathbf{I} \\ \boldsymbol{\Omega}^2 & 2\mathbf{Z}\boldsymbol{\Omega} \end{bmatrix}, \quad \hat{\mathbf{B}}_1 = \begin{bmatrix} \mathbf{0} \\ \mathbf{L_{w,m}} \end{bmatrix}, \quad \hat{\mathbf{B}}_2 = \begin{bmatrix} \mathbf{0} \\ \mathbf{L_{u,m}} \end{bmatrix},$$

$$\hat{\mathbf{C}}_1 = \begin{bmatrix} \mathbf{C_{zq,m}} & \mathbf{0} \\ \mathbf{0} & \mathbf{C_{zv,m}} \end{bmatrix}, \quad \hat{\mathbf{C}}_2 = [\mathbf{0}\ \ \mathbf{C_{yv,m}}].$$

Using an appropriate coordinate transformation [12], Expression (3) can be converted to the first modal state space form as

$$\begin{aligned} \dot{\mathbf{x}}_\mathbf{m} &= \mathbf{A_m}\mathbf{x_m} + \mathbf{B_m}1\mathbf{d} + \mathbf{B_{m2}}\mathbf{u}, \\ \mathbf{z} &= \mathbf{C_{m1}}\mathbf{x_m}, \\ \mathbf{y} &= \mathbf{C_{m2}}\mathbf{x_m}, \end{aligned} \tag{4}$$

where the state matrix is

$$\mathbf{A_m} = \mathrm{diag}\left\{ \begin{pmatrix} 0 & \omega_1 \\ -\omega_1 & -2\zeta_1\omega_1 \end{pmatrix} \cdots \begin{pmatrix} 0 & \omega_N \\ -\omega_N & -2\zeta_N\omega_N \end{pmatrix} \right\}. \tag{5}$$

2.1. Signal weightings for the best location selection

Most often in control engineering, it is necessary to emphasize some of the desired control objectives and also some re-scalings of the inputs and outputs is required (Fig. 1). This is done by using the signal weightings as shown in Fig. 2. Some measurement noise is also modeled.

In Fig. 2, each system ($\mathbf{W}_{\text{dist}}, \mathbf{W}_{\text{sn}}, \mathbf{W}_{\text{er}}, \mathbf{W}_{\text{in}}$ and **Plant**) has its own state space realization. If these subsystems are interconnected, the generalized plant in Fig. 2 has the state space representation

$$\dot{\mathbf{x}} = \mathbf{A}_g\mathbf{x}_g + \mathbf{B}_{g_1}\mathbf{w} + \mathbf{B}_{g_2}\mathbf{u},$$

$$\mathbf{z} = \mathbf{C}_{g_1}\mathbf{x}_g + \mathbf{D}_{g_{11}}\mathbf{w} + \mathbf{D}_{g_{12}}\mathbf{u},$$

$$\mathbf{y} = \mathbf{C}_{g_2}\mathbf{x}_g + \mathbf{D}_{g_{21}}\mathbf{w} + \mathbf{D}_{g_{22}}\mathbf{u}, \tag{6}$$

where $\mathbf{w}$, $\mathbf{z}$ and $\mathbf{y}$ are $[\mathbf{d}^{\mathrm{T}}\ \mathbf{n}^{\mathrm{T}}]^{\mathrm{T}}$, $[\mathbf{e}^{\mathrm{T}}\ \mathbf{u}_{\mathbf{m}}^{\mathrm{T}}]^{\mathrm{T}}$ and $\mathbf{y}_{\mathbf{m}}$, respectively.

2.2. Obtaining modal models of the generalized plant

Hiramoto et al. [10] designs their controller for the physical plant and neglect damping. Since in our work we aim to design a coprime controller for the plant shaped with signal weightings and keep the modal damping, we need to put the generalized plant into a modal state space form, where the state matrix is block diagonal and each mode can be dealt individually.

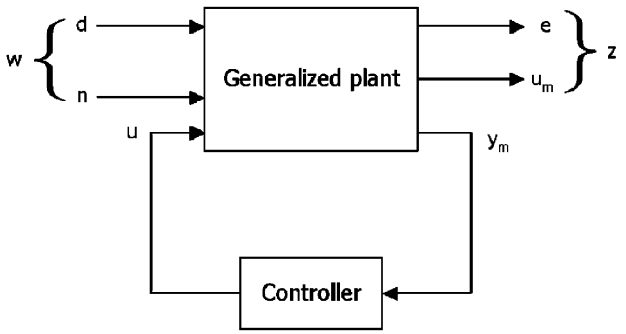

Fig. 1. The generalized control configuration.

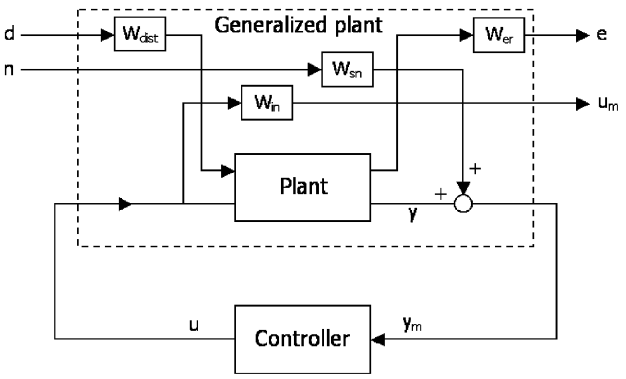

Fig. 2. The weighted generalized plant with the controller.

In Expression (6), $\mathbf{A}_g$, $\mathbf{B}_{g_1}$, $\mathbf{B}_{g_2}$, $\mathbf{C}_{g_1}$, $\mathbf{C}_{g_2}$, $\mathbf{D}_{g_{11}}$, $\mathbf{D}_{g_{12}}$, $\mathbf{D}_{g_{21}}$ and $\mathbf{D}_{g_{22}}$ are:

$$\mathbf{A}_g = \begin{bmatrix} \mathbf{A_m} & \mathbf{B_{m1}C_w} & \mathbf{0} & \mathbf{0} & \mathbf{0} \\ \mathbf{0} & \mathbf{A_w} & \mathbf{0} & \mathbf{0} & \mathbf{0} \\ \mathbf{B_zC_{m1}} & \mathbf{B_zD_{m11}C_w} & \mathbf{A_z} & \mathbf{0} & \mathbf{0} \\ \mathbf{0} & \mathbf{0} & \mathbf{0} & \mathbf{A_u} & \mathbf{0} \\ \mathbf{0} & \mathbf{0} & \mathbf{0} & \mathbf{0} & \mathbf{A_s} \end{bmatrix},$$

$$\mathbf{B}_{1g} = \begin{bmatrix} \mathbf{B_{m1}D_w} & \mathbf{0} \\ \mathbf{B_w} & \mathbf{0} \\ \mathbf{B_zD_{m11}D_w} & \mathbf{0} \\ \mathbf{0} & \mathbf{0} \\ \mathbf{0} & \mathbf{B_s} \end{bmatrix},$$

$$\mathbf{B}_{2g} = [\mathbf{B}_{\mathbf{m2}}^{\mathrm{T}} \ \mathbf{0} \ (\mathbf{B_zD_{m12}})^{\mathrm{T}} \ \mathbf{B}_{\mathbf{u}}^{\mathrm{T}} \ \mathbf{0}]^{\mathrm{T}},$$

$$\mathbf{C}_{1g} = \begin{bmatrix} \mathbf{0} & \mathbf{0} & \mathbf{0} & \mathbf{C_u} & 0 \\ \mathbf{D_zC_{m1}} & \mathbf{D_zD_{m11}C_w} & \mathbf{C_z} & \mathbf{0} & \mathbf{0} \end{bmatrix},$$

$$\mathbf{C}_{2g} = -[\mathbf{C_{m2}} \ \mathbf{D_{m21}C_w} \ \mathbf{0} \ \mathbf{0} \ \mathbf{C_s}],$$

$$\mathbf{D}_{11g} = \begin{bmatrix} \mathbf{0} & \mathbf{0} \\ \mathbf{D_zD_{m11}D_w} & \mathbf{0} \end{bmatrix},$$

$$\mathbf{D}_{12g} = \begin{bmatrix} \mathbf{D_u} \\ \mathbf{D_zD_{m12}} \end{bmatrix},$$

$$\mathbf{D}_{21g} = -[\mathbf{D_{m21}D_w} \ \mathbf{D_s}],$$

$$\mathbf{D}_{22g} = -\mathbf{D_{m22}}. \tag{7}$$

Using a coordinate transformation the global state matrix $\mathbf{A}_g$ can be put into a block diagonal form as

$$\mathbf{A} = \mathrm{blockdiag}\{\mathbf{A_m}, \ \mathbf{A_w}, \ \mathbf{A_z}, \ \mathbf{A_u}, \ \mathbf{A_s}\}. \tag{8}$$

This form of the state matrix will enable us to obtain simple and approximate solutions of the AREs in the controller synthesis step.

Since the eigenvalues of the global state matrices in Eqs. (7) and (8) are equal, there exists a single diagonal eigenvalue matrix $\mathbf{\Lambda}$ for both of the state matrices in Eqs. (7) and (8) which obey

$$\mathbf{A}_g = \mathbf{X\Lambda X}^{-1},$$

$$\mathbf{A} = \hat{\mathbf{X}}\mathbf{\Lambda}\hat{\mathbf{X}}^{-1},$$

where $\mathbf{\Lambda} = \mathrm{diag}\{\lambda_1, \lambda_2, \ldots \lambda_i, \ldots \lambda_n\}$.

Hence, the state matrix in Eq. (7) can be easily put into the form in Eq. (8) by the coordinate transformation $\hat{\mathbf{x}} = \mathbf{Zx}$, where $\mathbf{Z} = \hat{\mathbf{X}}^{-1}\mathbf{X}$. The obtained state space matrices are:

$$\begin{aligned} \mathbf{A} &= \mathbf{Z}^{-1}\mathbf{A}_g\mathbf{Z}, \\ \mathbf{B}_1 &= \mathbf{B}_{1g}\mathbf{Z}, \quad \mathbf{B}_2 = \mathbf{B}_{2g}\mathbf{Z}, \\ \mathbf{C}_1 &= \mathbf{Z}^{-1}\mathbf{C}_{g1}, \quad \mathbf{C}_2 = \mathbf{Z}^{-1}\mathbf{C}_{g_2}, \\ \mathbf{D}_{11} &= \mathbf{D}_{g11}, \quad \mathbf{D}_{12} = \mathbf{D}_{g12}, \\ \mathbf{D}_{21} &= \mathbf{D}_{g21}, \quad \mathbf{D}_{22} = \mathbf{D}_{g22}. \end{aligned} \tag{9}$$

3. Controller design

Since most controller design methods are time consuming, the location selection problem becomes computationally complex. Therefore, most optimal location selection methods try to bypass the controller design step. Hence, if one desires to apply a closed-loop location selection method, the controller design part should not take much computation time. For this purpose Hiramoto et al. [10] suggest a simple controller design procedure. They obtain a coprime controller for the lower part of the generalized plant $\mathbf{P_{yu}}$, by manipulating the corresponding generalized ARE such that it has a predefinite simple solution. The robust coprime controller design Hiramoto et al. [10] has developed is a modified version of the robust stabilization of coprime factors [2,11].

3.1. Controller used by Hiramoto et al. [10]

Hiramoto et al. [10] augment the plant $\mathbf{P_{yu}}$ as $\mathbf{P}_a = \alpha\mathbf{P_{yu}}$ and obtain a feedback controller $\mathbf{K}_a$ (see Fig. 3), where α serves as a design parameter and β is used to obtain suboptimal controller by selecting β slightly greater than one. For improving disturbance rejection properties of a controller, one should increase α. However, for obtaining the robustness of the closed-loop system, α should be kept as small as possible. Hence, there is a tradeoff for this parameter as discussed detailed in Hiramoto et al. [10]. In Fig. 3, the $\mathbf{P_{yu}}$ has the state space realization

$$\mathbf{P_{yu}} = \left[\begin{array}{c|c} \mathbf{A} & \mathbf{B}_2 \\ \hline \mathbf{C}_2 & \mathbf{0} \end{array}\right]. \tag{10}$$

The controller that is used in the optimization part of Ref. [10] is $K_\infty = \alpha K_a$ and K_a is obtained by solving the ARE of the augmented plant P_a:

$$\mathbf{A}^{\mathrm{T}}\mathbf{S} + \mathbf{S}\mathbf{A} - \alpha^2\mathbf{S}\mathbf{B}_2\mathbf{B}_2^{\mathrm{T}}\mathbf{S} + \mathbf{C}_2^{\mathrm{T}}\mathbf{C}_2 = 0, \tag{11}$$

$$\mathbf{A}\mathbf{T} + \mathbf{T}\mathbf{A}^{\mathrm{T}} - \mathbf{T}\mathbf{C}_2^{\mathrm{T}}\mathbf{C}_2\mathbf{T} + \alpha^2\mathbf{B}_2\mathbf{B}_2^{\mathrm{T}} = 0. \tag{12}$$

The diagonal positive-definite matrices

$$\mathbf{S} = \mathrm{diag}\{s_1, s_1, s_2, s_2, \ldots, s_N, s_N\}, \tag{13}$$

$$\mathbf{T} = \mathrm{diag}\{t_1, t_1, t_2, t_2, \ldots, t_N, t_N\}, \tag{14}$$

are assumed as the solutions of the Eqs. (11) and (12).

To obtain Expressions (13) and (14), Hiramoto et al. [10] neglect the modal damping for all modes and solve the simplified AREs (11) and (12) for zero-damping state space matrices. However, in our study we keep the damping, add new signal weights to the generalized plant and still obtain approximate ARE solutions, which lead to simple but more efficient $\mathscr{H}_\infty$ controller design.

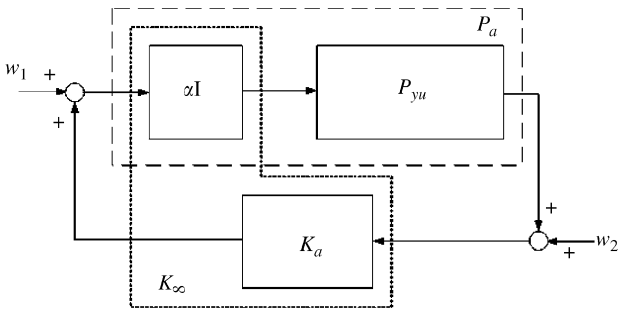

Fig. 3. Closed-loop system with P_{yu} and $\mathscr{H}_\infty$ controller [10].

3.2. Improved coprime controller

The approximate solutions of Eqs. (11) and (12) can be determined using the following property: controllability and observability Gramians of diagonally dominant state matrices are also diagonally dominant and their off-diagonal terms can be neglected [12]. Hence, for state space realizations in one of the modal forms [12], one can solve the generalized ARE in Eqs. (11) and (12) approximately.

The Gramians are used to express the controllability and observability properties of a system qualitatively and are defined as [13]

$$\mathbf{W}_c(t) = \int_0^t \exp(\mathbf{A}t)\mathbf{B}\mathbf{B}^{\mathrm{T}} \exp(\mathbf{A}^{\mathrm{T}}t)\,\mathrm{d}t,$$

$$\mathbf{W}_o(t) = \int_0^t \exp(\mathbf{A}t)\mathbf{C}^{\mathrm{T}}\mathbf{C} \exp(\mathbf{A}^{\mathrm{T}}t)\,\mathrm{d}t.$$

The exact (full) controllability and observability Gramians are obtained alternatively from the Lyapunov equations

$$\mathbf{A}\mathbf{W}_c + \mathbf{W}_c\mathbf{A}^{\mathrm{T}} + \mathbf{B}\mathbf{B}^{\mathrm{T}} = 0,$$

$$\mathbf{A}^{\mathrm{T}}\mathbf{W}_o + \mathbf{W}_o\mathbf{A} + \mathbf{C}^{\mathrm{T}}\mathbf{C} = 0.$$

The generalized plant has N modes. The first N_p modes are the physical modes and the remaining N_w modes are relating the signal weights. For the first ith modes ($i = 1$ to N), the Lyapunov equations simplify to

$$w_{ci}(\mathbf{A}_i + \mathbf{A}_i^{\mathrm{T}}) + \mathbf{B}_i\mathbf{B}_i^{\mathrm{T}} = 0, \tag{15}$$

$$w_{oi}(\mathbf{A}_i + \mathbf{A}_i^{\mathrm{T}}) + \mathbf{C}_i^{\mathrm{T}}\mathbf{C}_i = 0, \tag{16}$$

where

$$\mathbf{A}_i = \begin{bmatrix} 0 & \omega_i \\ -\omega_i & -2\zeta_i\omega_i \end{bmatrix},$$

$$\mathbf{B}_i\mathbf{B}_i^{\mathrm{T}} = \begin{bmatrix} 0 & 0 \\ 0 & \|\mathbf{B}_i\|_2^2 \end{bmatrix}, \quad \|\mathbf{B}_i\|_2^2 = (b_{i1}^2 + b_{i2}^2 + \cdots + b_{iN_u}^2),$$

$$\mathbf{C}_i^{\mathrm{T}}\mathbf{C}_i = \begin{bmatrix} 0 & 0 \\ 0 & \|\mathbf{C}_i\|_2^2 \end{bmatrix}, \quad \|\mathbf{C}_i\|_2^2 = (c_{i1}^2 + c_{i2}^2 + \cdots + c_{iN_u}^2).$$

$\mathbf{B}_i$ is the ith mode's contribution to the input matrix

$$\mathbf{B} = \begin{bmatrix} 0 & 0 & \cdots & 0 \\ b_{11} & b_{12} & \cdots & b_{1N_u} \\ 0 & 0 & \cdots & 0 \\ b_{21} & b_{21} & \cdots & b_{2N_u} \\ \vdots & & & \vdots \\ 0 & 0 & \cdots & 0 \\ b_{N1} & b_{N2} & \cdots & b_{NN_u} \end{bmatrix} \tag{17}$$

and $\mathbf{C}_i$ is the ith mode's contribution to the output matrix

$$\mathbf{C} = \begin{bmatrix} 0 & c_{11} & 0 & c_{21} & \cdots & 0 & c_{N1} \\ 0 & c_{12} & 0 & c_{22} & & 0 & c_{N2} \\ \vdots & \vdots & & \vdots & & \vdots & \vdots \\ 0 & c_{1N_s} & 0 & c_{2N_s} & \cdots & 0 & c_{NN_s} \end{bmatrix}. \tag{18}$$

So, if $\mathbf{A}_i$, $\mathbf{B}_i$ and $\mathbf{C}_i$ are inserted into Eqs. (15) and (16), the approximate controllability and observability Gramians for the ith mode are:

$$w_{ci} \cong \frac{\|\mathbf{B}_i\|_2^2}{4\zeta_i\omega_i}, \tag{19}$$

$$w_{oi} \cong \frac{\|\mathbf{C}_i\|_2^2}{4\zeta_i\omega_i}. \tag{20}$$

If only ith mode is considered, AREs (11) and (12) become

$$\mathbf{A}_i^{\mathrm{T}} s_i I_2 + s_i I_2 \mathbf{A}_i - \alpha^2 s_i I_2 \mathbf{B}_i \mathbf{B}_i^{\mathrm{T}} s_i I_2 + \mathbf{C}_i^{\mathrm{T}} \mathbf{C}_i = 0,$$

$$\mathbf{A}_i t_i I_2 + t_i I_2 \mathbf{A}_i^{\mathrm{T}} - t_i I_2 \mathbf{C}_i^{\mathrm{T}} \mathbf{C}_i t_i I_2 + \alpha^2 \mathbf{B}_i \mathbf{B}_i^{\mathrm{T}} = 0,$$

which can be expressed as

$$s_i(\mathbf{A}_i^{\mathrm{T}} + \mathbf{A}_i) - \alpha^2 s_i^2 \mathbf{B}_i \mathbf{B}_i^{\mathrm{T}} + \mathbf{C}_i^{\mathrm{T}} \mathbf{C}_i = 0, \tag{21}$$

$$t_i(\mathbf{A}_i + \mathbf{A}_i^{\mathrm{T}}) - t_i^2 \mathbf{C}_i^{\mathrm{T}} \mathbf{C}_i + \alpha^2 \mathbf{B}_i \mathbf{B}_i^{\mathrm{T}} = 0. \tag{22}$$

Since it is clear from Eqs. (15) and (16) that

$$\mathbf{B}_i \mathbf{B}_i^{\mathrm{T}} = -w_{ci}(\mathbf{A}_i + \mathbf{A}_i^{\mathrm{T}}),$$

$$\mathbf{C}_i^{\mathrm{T}} \mathbf{C}_i = -w_{oi}(\mathbf{A}_i + \mathbf{A}_i^{\mathrm{T}}),$$

where

$$\mathbf{A}_i + \mathbf{A}_i^{\mathrm{T}} = \begin{bmatrix} 0 & 0 \\ 0 & -4\zeta_i\omega_i \end{bmatrix},$$

Eqs. (21) and (22) become scalar quadratic equations of s_i and t_i as

$$s_i^2 \alpha^2 w_{ci} + s_i - w_{oi} = 0,$$

$$t_i^2 w_{oi} + t_i - \alpha^2 w_{ci} = 0.$$

Since the solutions of Eqs. (11) and (12) must be positive definite ($s_i > 0$ and $t_i > 0$), the positive solutions of the scalar quadratic equations

$$s_i = \frac{-1 + \sqrt{1 + 4\alpha^2 w_{ci} w_{oi}}}{2\alpha^2 w_{ci}}, \tag{23}$$

$$t_i = \frac{-1 + \sqrt{1 + 4\alpha^2 w_{ci} w_{oi}}}{2w_{oi}} \tag{24}$$

are taken as the approximate solutions of the control and filter AREs.

For each of the N_w modes from $i = N_p + 1$ to N, which are concerned with signal weights, the Gramians are:

$$w_{ci}^w(a_i + a_i^{\mathrm{T}}) + \mathbf{b}_i \mathbf{b}_i^{\mathrm{T}} = 0, \tag{25}$$

$$w_{oi}^{w}(a_i + a_i^{\mathrm{T}}) + \mathbf{b}_i^{\mathrm{T}}\mathbf{b}_i = 0. \tag{26}$$

Here a_i is scalar and is ith mode's contribution to the global block diagonalized state matrix $\mathbf{A}$. $\mathbf{b}_i\mathbf{b}_i^{\mathrm{T}}$ and $\mathbf{c}_i^{\mathrm{T}}\mathbf{c}_i$ are:

$$\mathbf{b}_i\mathbf{b}_i^{\mathrm{T}} = \|\mathbf{b}_i\|_2^2 = (b_{i1}^2 + b_{i2}^2 + \cdots + b_{iN_u}^2),$$

$$\mathbf{c}_i^{\mathrm{T}}\mathbf{c}_i = \|\mathbf{c}_i\|_2^2 = (c_{i1}^2 + c_{i2}^2 + \cdots + c_{iN_u}^2).$$

$\mathbf{b}_i$ is the ith mode's contribution to the input matrix

$$\mathbf{b} = \begin{bmatrix} b_{11} & b_{12} & \cdots & b_{1N_u} \\ b_{21} & b_{21} & \cdots & b_{2N_u} \\ \vdots & & & \vdots \\ b_{N_w1} & b_{N_w2} & \cdots & b_{N_wN_u} \end{bmatrix}$$

and $\mathbf{c}_i$ is the ith mode's contribution to the output matrix

$$\mathbf{c} = \begin{bmatrix} c_{11} & c_{21} & \cdots & c_{N_w1} \\ c_{12} & c_{22} & & c_{N_w2} \\ \vdots & \vdots & & \vdots \\ c_{1N_s} & c_{2N_s} & \cdots & c_{N_wN_s} \end{bmatrix}.$$

The first $2 \times N_p$ entries of the diagonal approximate Gramian are calculated from Eqs. (19) and (20). The remaining N_w entries of the Gramian are calculated from Eqs. (25) and (26) as follows:

$$w_{ci}^{w} \cong -\frac{\mathbf{b}_i\mathbf{b}_i^{\mathrm{T}}}{2a_i}, \quad i = 1 : N_w,$$

$$w_{oi}^{w} \cong -\frac{\mathbf{c}_i^{\mathrm{T}}\mathbf{c}_i}{2a_i}, \quad i = 1 : N_w.$$

The controllability and observability Gramians of the weighted generalized plant can be obtained approximately as

$$\mathrm{W}_c = \mathrm{diag}\{w_{c1}, w_{c1}, w_{c2}, w_{c2}, \ldots w_{cN_p}, w_{cN_p}, w_{c1}^{w}, w_{c2}^{w}, \ldots w_{cN_w}^{w}\}, \tag{27}$$

$$\mathrm{W}_o = \mathrm{diag}\{w_{o1}, w_{o1}, w_{o2}, w_{o2}, \ldots w_{oN_p}, w_{oN_p}, w_{o1}^{w}, w_{o2}^{w}, \ldots w_{oN_w}^{w}\}. \tag{28}$$

The solutions of Eqs. (21) and (22) for the weighting modes from $N_p + 1$ to $N = N_p + N_w$ have the same expressions as s_i and t_i in Eqs. (23) and (24). Hence, once the Gramians in Expressions (27) and (28) are calculated, the solutions of AREs for the generalized plant can be obtained directly from Eqs. (23) and (24).

The controller K_∞ in Fig. 3 is obtained by solving the Riccati equations (11) and (12) approximately and by choosing the parameters $\alpha > 0$, $\beta > 1$. With the controller K_∞, the state space realization of the closed-loop system $\mathbf{G_{zw}}(s)$ is

$$\dot{\mathbf{x}}_c = \mathbf{A}_c\mathbf{x}_c + \mathbf{B}_c\mathbf{w}, \tag{29}$$

$$\mathbf{z}_c = \mathbf{C}_c\mathbf{x}_c, \tag{30}$$

where

$$\mathbf{x}_c = \begin{bmatrix} \mathbf{x} \\ \mathbf{x}_{\mathbf{K}_a} \end{bmatrix}, \quad \mathbf{A}_c = \begin{bmatrix} \mathbf{A} & \alpha\mathbf{B}_2(\mathbf{L_u})\mathbf{C}_{\mathbf{K}_a}(\mathbf{L_u}) \\ \mathbf{B}_{\mathbf{K}_a}(\mathbf{L_u})\mathbf{C}_2(\mathbf{L_u}) & \mathbf{A}_{\mathbf{K}_a}(\mathbf{L_u}) \end{bmatrix},$$

$$\mathbf{B}_c = [\mathbf{B}_1^{\mathrm{T}} \ \mathbf{0}]^{\mathrm{T}}, \quad \mathbf{C}_c = [\mathbf{C}_1 \ \ \alpha\mathbf{D}_{12}\mathbf{C}_{\mathbf{K}_a}].$$

$\mathbf{A}_{\mathbf{K}_a}$, $\mathbf{B}_{\mathbf{K}_a}$ and $\mathbf{C}_{\mathbf{K}_a}$ are the state space matrices of the controller in Fig. 3 and have the expressions

$$\begin{aligned}\mathbf{A}_{\mathbf{K}_a} &= \mathbf{A} - \alpha\mathbf{B}_2\mathbf{B}_2^{\mathrm{T}}\mathbf{S} + (\beta\gamma_{\min})^2(\mathbf{W}^{-1})^{\mathrm{T}}\mathbf{T}\mathbf{C}_2^{\mathrm{T}}\mathbf{C}_2,\\ \mathbf{B}_{\mathbf{K}_a} &= (\beta\gamma_{\min})^2(\mathbf{W}^{-1})^{\mathrm{T}}\mathbf{T}\mathbf{C}_2^{\mathrm{T}},\\ \mathbf{C}_{\mathbf{K}_a} &= \alpha\mathbf{B}_2^{\mathrm{T}}\mathbf{S},\end{aligned} \tag{31}$$

$$\text{with}\quad \mathbf{W} = (1-(\beta\gamma_{\min})^2)\mathbf{I} + \mathbf{S}\mathbf{T},\quad \gamma_{\min} = (\mathbf{I} + \lambda_{\max}(\mathbf{S}\mathbf{T}))^{1/2}.$$

$\lambda_{\max}(.)$ is the maximum eigenvalue. The closed-loop system $\mathbf{G}_{\mathbf{zw}}(s)$ includes open-loop plant and controller matrices which are functions of the configuration of the actuators and sensors.

4. Optimization of the actuator and sensor locations

The problem of optimal placement of the actuators and sensors can stated as follows: Given the closed-loop system with the state space representation in Eqs. (29) and (30), find the actuator/sensor placement matrix $\mathbf{L}_{\mathbf{u}}$, which minimizes the optimization metric that is chosen by the designer.

The $\mathscr{H}_2$ norm of the closed-loop system is selected as the optimization criterion for the optimal placement as in the approach developed by Hiramoto et al. [10]. However, since they design their controller for the physical system without any signal weightings and neglect the damping, they solve AREs simply and do not need the derivatives of AREs.

Unlike their controller design technique, we use the signal weightings and the damping. So, the partial derivatives of AREs in Eqs. (11) and (12) are required to obtain the gradient of the objective function. Hence, in this section the partial derivatives of approximate ARE solutions are introduced as another significant contribution.

4.1. Selection of the objective function

The optimization metric J which is the square of the $\mathscr{H}_2$-norm can be given as

$$J = \|\mathbf{G}_{\mathbf{zw}}\|_2^2 = \mathrm{trace}(\mathbf{C}_c\mathbf{L}_c\mathbf{C}_c^{\mathrm{T}}), \tag{32}$$

where $\mathbf{L}_c$ is the controllability Gramian of the closed-loop system and satisfies the equation

$$\mathbf{A}_c\mathbf{L}_c + \mathbf{L}_c\mathbf{A}_c^{\mathrm{T}} + \mathbf{B}_c\mathbf{B}_c^{\mathrm{T}} = 0. \tag{33}$$

Since the optimization function J is partially differentiable with respect to the locations ξ_a^i, a gradient descent method can be applied to obtain the optimal locations of the collocated actuator/sensor pairs [14].

If the location of the ith actuator/sensor pair is given by the coordinate ξ_a^i, the partial derivative of J in Eq. (32) with respect to ξ_a^i is

$$\frac{\partial J}{\partial \xi_a^i} = \mathrm{trace}\left(\frac{\partial \mathbf{C}_c}{\partial \xi_a^i}\mathbf{L}_c\mathbf{C}\mathbf{c}^{\mathrm{T}} + \mathbf{C}_c\frac{\partial \mathbf{L}_c}{\partial \xi_a^i}\mathbf{C}\mathbf{c}^{\mathrm{T}} + \mathbf{C}_c\mathbf{L}_c\frac{\partial \mathbf{C}\mathbf{c}^{\mathrm{T}}}{\partial \xi_a^i}\right) \tag{34}$$

where $\partial\mathbf{C}_c/\partial\xi_a^i$ is

$$\frac{\partial \mathbf{C}_c}{\partial \xi_a^i} = \left[\frac{\partial \mathbf{C}_1}{\partial \xi_a^i} \quad \alpha\mathbf{D}_{12}\frac{\partial \mathbf{C}_{\mathbf{K}_a}}{\partial \xi_a^i}\right].$$

$\partial\mathbf{L}_c/\partial\xi_a^i$ in Eq. (34) is to be obtained by the equation that is achieved by differentiating Eq. (33) with respect to the actuator/sensor locations ξ_a^i as

$$\mathbf{A}_c\mathbf{Y} + \mathbf{Y}\mathbf{A}_c^{\mathrm{T}} + \mathbf{Q} = 0,$$

where

$$\mathbf{Y} = \frac{\partial \mathbf{L}_c}{\partial \xi_a^i},\quad \mathbf{Q} = \frac{\partial \mathbf{A}_c}{\partial \xi_a^i}\mathbf{L}_c + \mathbf{L}_c\frac{\partial \mathbf{A}_c^{\mathrm{T}}}{\partial \xi_a^i} + \frac{\partial \mathbf{B}_c}{\partial \xi_a^i}\mathbf{B}_c^{\mathrm{T}} + \mathbf{B}_c\frac{\partial \mathbf{B}_c^{\mathrm{T}}}{\partial \xi_a^i}$$

$\partial \mathbf{A}_c/\partial \xi_a^i$ is simply the derivative of the state matrix of the closed-loop system with respect to ξ_a^i

$$\frac{\partial \mathbf{A}_c}{\partial \xi_a^i} = \begin{bmatrix} \mathbf{0} & \alpha\left(\dfrac{\partial \mathbf{B}_2}{\partial \xi_a^i} + \dfrac{\partial \mathbf{C}_{\mathbf{K}_a}}{\partial \xi_a^i}\right) \\ \dfrac{\partial \mathbf{B}_{\mathbf{K}_a}}{\partial \xi_a^i}\mathbf{C}_2 + \mathbf{B}_{\mathbf{K}_a}\dfrac{\partial \mathbf{C}_2}{\partial \xi_a^i} & \dfrac{\partial \mathbf{A}_{\mathbf{K}_a}}{\partial \xi_a^i} \end{bmatrix},$$

where $(\partial \mathbf{A}_{\mathbf{K}_a}/\partial \xi_a^i, \partial \mathbf{B}_{\mathbf{K}_a}/\partial \xi_a^i, \partial \mathbf{C}_{\mathbf{K}_a}/\partial \xi_a^i)$ are the derivatives of the controller matrices in Eqs. (31), which are functions of the open-loop generalized plant in Eqs. (9). So, to compute $\partial \mathbf{A}_c/\partial \xi_a^i$, the derivatives of Eqs. (9) are required. In Eq. (9), $\mathbf{Z}$ is made of the eigenvectors of the state matrices $\mathbf{A}$ and $\mathbf{A}_g$. Since the natural frequencies and the signal weightings do not change with actuator/sensor locations, the eigenvector $\hat{\mathbf{X}}$ associated with $\hat{\mathbf{A}}$ and the eigenvector $\mathbf{X}$ of $\mathbf{A}$ can be assumed to have zero partial derivatives. Hence, for calculating the derivatives of Eqs. (9), one should differentiate only the terms, which are functions of $\mathbf{L_u}$ in Eqs. (7). These terms are $\mathbf{B_{m2}}, \mathbf{C_{m1}}, \mathbf{C_{m2}}$ in Eqs. (4).

4.2. Approximate ARE derivatives

In Hiramoto et al. [10], the solutions of AREs, denoted by $\mathbf{S}$ and $\mathbf{T}$, do not contribute to the partial derivatives of the closed-loop system. However, the solutions of AREs for the improved coprime controller introduced in Section 3.2 have partial derivatives with respect to the actuator and sensor locations.

The derivatives of AREs (11) and (12) with respect to design parameters p, which are the coordinates of the actuator/sensor pairs $(\xi_a^1 \ldots \xi_a^{N_u})$, are:

$$(\mathbf{A}^{\mathrm{T}} - \alpha^2 \mathbf{S}\mathbf{B}_2\mathbf{B}_2^{\mathrm{T}})\frac{\partial \mathbf{S}}{\partial p} + \frac{\partial \mathbf{S}}{\partial p}(\mathbf{A} - \alpha^2 \mathbf{S}\mathbf{B}_2^{\mathrm{T}}\mathbf{B}_2) + Q = 0, \tag{35}$$

$$(\mathbf{A} - \mathbf{T}\mathbf{C}_2^{\mathrm{T}}\mathbf{C}_2)\frac{\partial \mathbf{T}}{\partial p} + \frac{\partial \mathbf{T}}{\partial p}(\mathbf{A}^{\mathrm{T}} - \mathbf{T}\mathbf{C}_2^{\mathrm{T}}\mathbf{C}_2) + P = 0, \tag{36}$$

where Q and P are:

$$Q = \frac{\partial \mathbf{A}^{\mathrm{T}}}{\partial p}\mathbf{S} + \mathbf{S}\frac{\partial \mathbf{A}}{\partial p} - \alpha^2 \mathbf{S}\frac{\partial \mathbf{B}_2}{\partial p}\mathbf{B}_2^{\mathrm{T}}\mathbf{S} - \alpha^2 \mathbf{S}\mathbf{B}_2\frac{\partial \mathbf{B}_2^{\mathrm{T}}}{\partial p}\mathbf{S} + \frac{\partial \mathbf{C}_2^{\mathrm{T}}}{\partial p}\mathbf{C}_2 + \mathbf{C}_2^{\mathrm{T}}\frac{\partial \mathbf{C}_2}{\partial p}$$

and

$$P = \frac{\partial \mathbf{A}}{\partial p}\mathbf{T} + \mathbf{T}\frac{\partial \mathbf{A}^{\mathrm{T}}}{\partial p} - \mathbf{T}\frac{\partial \mathbf{B}_2}{\partial p}\mathbf{B}_2^{\mathrm{T}}\mathbf{T} - \mathbf{T}\mathbf{B}_2\frac{\partial \mathbf{B}_2^{\mathrm{T}}}{\partial p}\mathbf{T} + \alpha^2\frac{\partial \mathbf{C}_2^{\mathrm{T}}}{\partial p}\mathbf{C}_2 + \alpha^2\mathbf{C}_2^{\mathrm{T}}\frac{\partial \mathbf{C}_2}{\partial p},$$

respectively.

Eqs. (35) and (36) are Lyapunov equations and their solutions are obtained in the same manner as in finding the solutions Eqs. (11) and (12). Since the system equations of the generalized plant is put into the first modal state space representation, Eqs. (35) and (36) can be solved for each mode separately. For the ith mode, they are:

$$(1 + 2\alpha^2 s_i w_{ci})4\zeta_i\omega_i\frac{\partial s_i}{\partial p} + s_i\frac{\partial}{\partial p}(4\zeta_i\omega_i) + \alpha^2 s_i^2\frac{\partial}{\partial p}((\mathbf{B}_{2_i}\mathbf{B}_{2_i}^{\mathrm{T}})_{(2,2)}) - \frac{\partial}{\partial p}((\mathbf{C}_{2_i}^{\mathrm{T}}\mathbf{C}_{2_i})_{(2,2)}) = 0, \tag{37}$$

$$(1 + 2t_i w_{oi})4\zeta_i\omega_i\frac{\partial t_i}{\partial p} + t_i\frac{\partial}{\partial p}(4\zeta_i\omega_i) + t_i^2\frac{\partial}{\partial p}((\mathbf{C}_{2_i}^{\mathrm{T}}\mathbf{C}_{2_i})_{(2,2)}) - \alpha^2\frac{\partial}{\partial p}((\mathbf{B}_{2_i}\mathbf{B}_{2_i}^{\mathrm{T}})_{(2,2)}) = 0, \tag{38}$$

where the partial derivatives of $(\mathbf{B}_{2_i}\mathbf{B}_{2_i}^{\mathrm{T}})_{(2,2)}$ and $(\mathbf{C}_{2_i}^{\mathrm{T}}\mathbf{C}_{2_i})_{(2,2)}$ are:

$$\frac{\partial}{\partial p}((\mathbf{B}_{2_i}\mathbf{B}_{2_i}^{\mathrm{T}})_{2,2}) = \frac{\partial}{\partial p}\|\mathbf{B}_{2_i}\|_2^2 = 2\left(b_{i1}\frac{\partial b_{i1}}{\partial p} + b_{i2}\frac{\partial b_{i2}}{\partial p} + \cdots + b_{iN_u}\frac{\partial b_{iN_u}}{\partial p}\right),$$

$$\frac{\partial}{\partial p}((\mathbf{C}_{2_i}^{\mathrm{T}}\mathbf{C}_{2_i})_{2,2}) = \frac{\partial}{\partial p}\|\mathbf{C}_{2_i}\|_2^2 = 2\left(c_{1i}\frac{\partial c_{1i}}{\partial p} + c_{2i}\frac{\partial c_{2i}}{\partial p} + \cdots + b_{iN_u}\frac{\partial c_{N_ui}}{\partial p}\right).$$

In Eqs. (37) and (38), the only unknown quantities are $\partial s_i/\partial p$ and $\partial t_i/\partial p$ and hence can be found immediately. So, the partial derivatives of $\mathbf{S}$ and $\mathbf{T}$ are

$$\frac{\partial \mathbf{S}}{\partial p} = \mathrm{diag}\left\{\frac{\partial s_1}{\partial p} \quad \cdots \quad \frac{\partial s_N}{\partial p}\right\},$$

$$\frac{\partial \mathbf{T}}{\partial p} = \mathrm{diag}\left\{\frac{\partial t_1}{\partial p} \quad \cdots \quad \frac{\partial t_N}{\partial p}\right\}.$$

4.3. Partial derivative of $\gamma_{\min}$

For taking the partial derivative of the closed-loop matrix $\mathbf{A}_c$ in Eq. (29) with respect to the design parameter p, the partial derivative of $\gamma_{\min}$ in Eq. (31) is also required.

$$\frac{\partial \gamma_{\min}}{\partial p} = \frac{1}{2\sqrt{\mathbf{I} + \lambda_{\max}(\mathbf{ST})}}\frac{\partial \lambda_{\max}(\mathbf{ST})}{\partial p},$$

where

$$\frac{\partial \lambda_{\max}(\mathbf{ST})}{\partial p} = u_k^{\mathrm{T}}\frac{\partial \mathbf{ST}}{\partial p}u_k,$$

k is the index of the maximum eigenvalue of $\mathbf{ST}$ as

$$\lambda_{\max} = \lambda_k = \max_i \lambda_i(\mathbf{ST}), \quad i = 1 : N_p$$

and u_k is the kth eigenvector of $\mathbf{ST}$.

The distinct eigenvalue derivative of $\partial\lambda_{\max}(.)/\partial p$ is taken according to Refs. [15,16].

4.4. Optimization procedure

Using the improved coprime controller design and the ARE derivatives, a gradient-based unconstrained optimization is utilized for the optimal location selection of point actuator and sensor pairs. The optimization procedure is done using the following steps:

(1) *Required data*: The disturbance locations, the boundary conditions and the dimensions of the structure is given.
(2) *Initial guess*: The initial guesses $(\xi_a^1 \ldots \xi_a^{N_u})$ are selected, where the objective function and its gradient will be evaluated. To be used in step size selection, some optimization parameters are chosen.
(3) *The physical structure modeling*: The structure is modeled and put into the first modal state space form ($\mathbf{A}_m$, $\mathbf{B}_{m1}$, $\mathbf{B}_{m2}$, $\mathbf{C}_{m1}$, $\mathbf{C}_{m2}$, $\mathbf{D}_{m11}$, $\mathbf{D}_{m12}$, $\mathbf{D}_{m21}$, $\mathbf{D}_{m22}$). The partial derivatives of the state space matrices $\mathbf{B}_{\mathbf{m}2}$, $\mathbf{C}_{\mathbf{m}1}$ and $\mathbf{C}_{\mathbf{m}2}$ are taken with respect to the current actuator and sensor locations.

(4) *The generalized plant*: For the given signal weightings the state space matrices of the shaped plant are obtained. Using the coordinate transformation it is put into to the first modal form with block diagonal state matrix ($\mathbf{A}$, $\mathbf{B}_1$, $\mathbf{B}_2$, $\mathbf{C}_1$, $\mathbf{C}_2$, $\mathbf{D}_{11}$, $\mathbf{D}_{12}$, $\mathbf{D}_{21}$, $\mathbf{D}_{22}$).
(5) *Controller synthesis and closed-loop system*: The AREs are solved and the coprime controller is obtained. The closed-loop state space matrices ($\mathbf{A}_c$, $\mathbf{B}_c$, $\mathbf{C}_c$, $\mathbf{D}_c$) are calculated.
(6) *Objective function and its gradient*: $\mathscr{H}_2$-norm is calculated and its square is set as the objective function J. The gradient of J is evaluated at the current actuator and sensor location.
(7) *The new actuator and sensor locations*: Using gradient of J, the search direction of the kth iterations is established as $s^k = \Delta x/\|\Delta x\|$ where Δx is given in Eq. (39). The next iterations's points become $x^{k+1} = x^k + ts^k$, with t being the step size. t is chosen according to the backtracking line search technique in Ref. [14]. If the difference $\|x^{k+1} - x^k\| < \varepsilon$, the optimization procedure is stopped. Otherwise, the procedure is returned to the second step with the next actuator and sensor points.

The negative gradient of the square of $\mathscr{H}_2$ norm of the closed-loop system in Eq. (32) is defined as

$$\Delta x \equiv -\begin{bmatrix} \dfrac{\partial J}{\partial \xi_a^1} \\ \vdots \\ \dfrac{\partial J}{\partial \xi_a^{N_u}} \end{bmatrix}, \tag{39}$$

where $\partial J/\partial \xi_a^i$ is calculated from Eq. (34).

5. Examples

As an example consider a simply supported Euler–Bernoulli beam shown in Fig. 4. ξ and ψ denote the horizontal coordinate and the vertical deflection, respectively. $w(t)$ and $u^i(t)$ with $i = 1, 2$ are the single disturbance and the two point actuator forces, respectively. The disturbance is located at ξ_w. The control forces from the first and the second actuators are acting at horizontal positions ξ_a^i for $i = 1, 2$. Since the rate sensors are collocated, they are at the same location as the actuators. The equation of motion and the boundary conditions are:

$$EI\frac{\partial^4\psi(\xi,t)}{\partial\xi^4} + \rho S\frac{\partial^2\psi(\xi,t)}{\partial t^2} = w(t)\delta(\xi-\xi_w) + \sum_{i=1}^{2} u^i(t)\delta(\xi-\xi_a^i)$$

$$\psi(0,t) = 0, \quad \psi(L,t) = 0, \quad \frac{\partial^2\psi(0,t)}{\partial\xi^2} = 0, \quad \frac{\partial^2\psi(L,t)}{\partial\xi^2} = 0. \tag{40}$$

EI, ρ, S and L are the flexural density, the density, cross-section area and the length of the beam, respectively. Their values are selected as: $E = 1\,\mathrm{Pa}$, $I = 1\,\mathrm{m}^4$, $\rho = 1\,\mathrm{kg\,m}^{-3}$, $S = 1\,\mathrm{m}^2$, $L = 1\,\mathrm{m}$. The parameters required

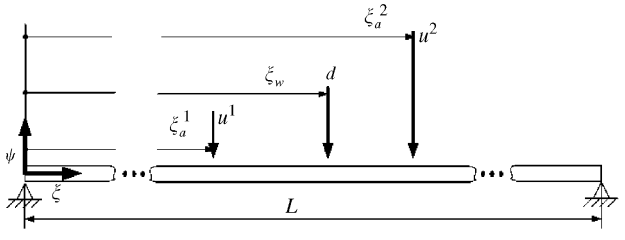

Fig. 4. Simply supported beam with two point control forces and a single disturbance.

for the controller design step are $\alpha = 100$, $\beta = 1.02$ and the performance outputs is described by the vector $z = [\psi(\xi_z^1), \psi(\xi_z^2), \psi(\xi_w), u^1, u^2]^{\mathrm{T}}$. Assumed modes method is used to discretize the problem. The number of modes are taken as $N = 10$. The damping for each mode is assumed to be $\zeta = 0.001$.

With the assumed modes approach, Eq. (40) can be solved by assuming the vertical displacement $\psi(\xi, t)$ to be of the following form:

$$\psi(\xi, t) = \sum_{i=1}^{N} q_i(t)\varphi_i(\xi),$$

$$\varphi_i(\xi) = \sqrt{\frac{2}{L}} \sin \frac{i\pi\xi}{L}, \tag{41}$$

where $q_i(t)$ and $\varphi_i(\xi)$ are the modal displacements and the normalized mode shapes, respectively. $\mathbf{L_w}$, $\mathbf{L_u}$ and the natural frequencies are:

$$\mathbf{L_w} = [\varphi_1(\xi_w) \;\; \varphi_2(\xi_w) \;\; \ldots \;\; \varphi_N(\xi_w)]^{\mathrm{T}},$$

$$\mathbf{L_u} = \begin{bmatrix} \varphi_1(\xi_a^1) & \varphi_2(\xi_a^1) & \ldots & \varphi_N(\xi_a^1) \\ \varphi_1(\xi_a^2) & \varphi_2(\xi_a^2) & \ldots & \varphi_N(\xi_a^2) \end{bmatrix}^{\mathrm{T}},$$

$$\omega_i = (i\pi)^2 \sqrt{\frac{EI}{\rho S L^4}} \quad \text{with } i = 1 : N, \quad \text{respectively.}$$

5.1. Optimal actuator and sensor locations for $\xi_w = 0.35L$

The single disturbance is located at the point $\xi_w = 0.35L$ and the initial places of the actuators are $\xi_a^1 = 0.25L$, $\xi_a^2 = 0.65L$.

The signal weightings of the generalized plant (in Fig. 2) have the transfer functions

$$\begin{aligned} W_{\mathrm{dist}} &= \frac{10}{0.03s + 1} \quad \text{(disturbance weight)}, \\ W_{\mathrm{sn}} &= \frac{1}{10^5} \quad \text{(sensor noise weight)}, \\ W_{\mathrm{er}} &= 1 \quad \text{(performance output weight)}, \\ W_{\mathrm{in}} &= \frac{1}{25} \quad \text{(control input weight)}. \end{aligned} \tag{42}$$

The resulting optimal actuator and sensor locations can be seen in Fig. 5. Starting from the initial locations $(0.25L, 0.65L)$, in nearly 55 iterations, the actuator/sensor pairs (ξ_a^1, ξ_a^2) converge to the final locations $(0.35L, 0.35L)$. The objective function $J = \mathscr{H}_2^2$ converges to its minimum also, as can be seen in Fig. 6.

To verify the obtained results, the $\mathscr{H}_2$-norm on the whole domain of the beam is calculated and the variation of J with the change in the actuator coordinates ξ_a^1 and ξ_a^2 is plotted in Figs. 7 and 8.

As can be seen in Figs. 7 and 8, there are actuator/sensor location pairs (ξ_a^1, ξ_a^2), for which the $\mathscr{H}_2$ norm are equivalent or very close.

Figs. 9 and 10 shows the results obtained by the formulation given in Hiramoto et al. [10]. That is, the damping is neglected. The disturbance input and sensor noise weightings are not present in this formulation. The obtained optimal locations with this formulation are given in Fig. 9 and the square of the $\mathscr{H}_2$-norm of the closed-loop system in Eq. (10) are different than those achieved in Figs. 5 and 6. Because of possibility of including weights and damping in the formulation, our formulation should give more realistic results.

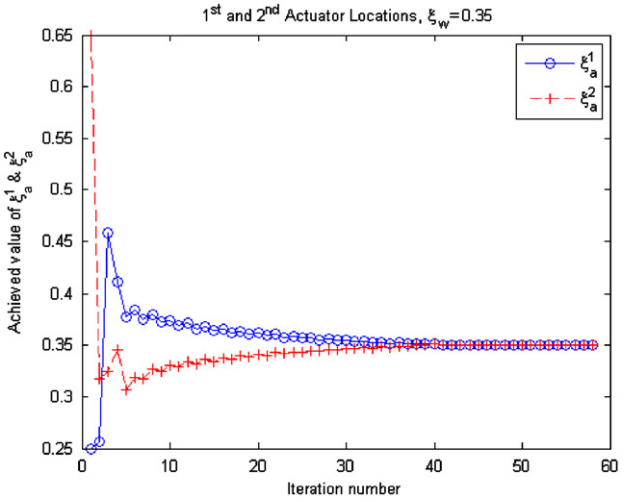

Fig. 5. Iterations and convergence to the optimum locations.

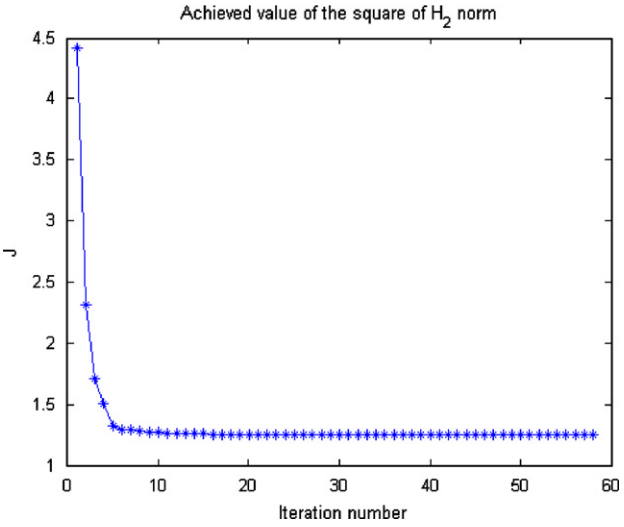

Fig. 6. Iterations and the minimized $\mathscr{H}_2^2$.

5.2. *Effect of the design parameter α and the filter coefficient* C_{W_w}

To see the effect of the signal weightings on the resulting optimal actuator/sensor locations, some parametric studies are done (Figs. 11–14). For simulations in Figs. 15–18, the initial points are $\xi_a^1 = 0.35L$ and $\xi_a^1 = 0.65L$. The disturbance force is located at $\xi_w = 0.5L$. The signal weightings and the parameter α for each simulation in Figs. 15–18 are listed in Table 1.

In Figs. 15–18, the, the minimized optimization metric J and the optimal actuator/sensor locations (ξ_a^1, ξ_a^2) are plotted versus the changing the parameter α and the coefficient C_{Ww} of a low-pass filter, which is interconnected to the physical plant.

In Fig. 15, as α increases, the square of the closed-loop $\mathscr{H}_2$-norm at the optimal actuator and sensor location decreases. Since the $\mathscr{H}_2$-norm is the norm of the closed-loop transfer function between the disturbance inputs and the performance outputs, for the disturbance rejection purpose α need to be selected as

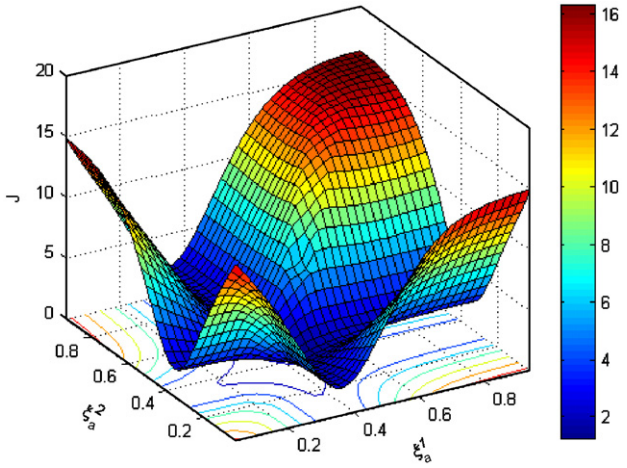

Fig. 7. The minimized $J = \mathscr{H}_2^2$ versus actuator locations.

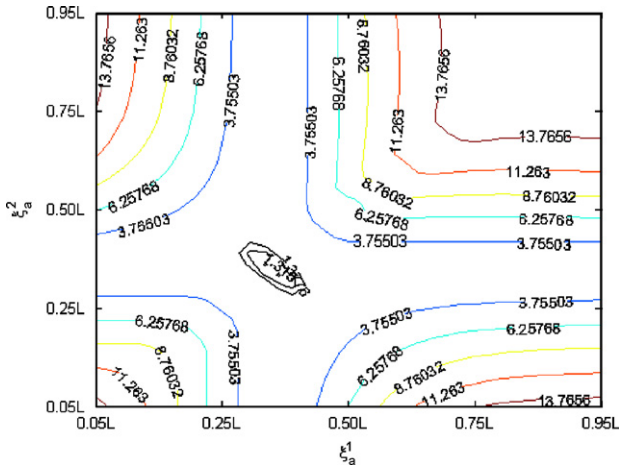

Fig. 8. The minimized $J = \mathscr{H}_2^2$ versus actuator locations.

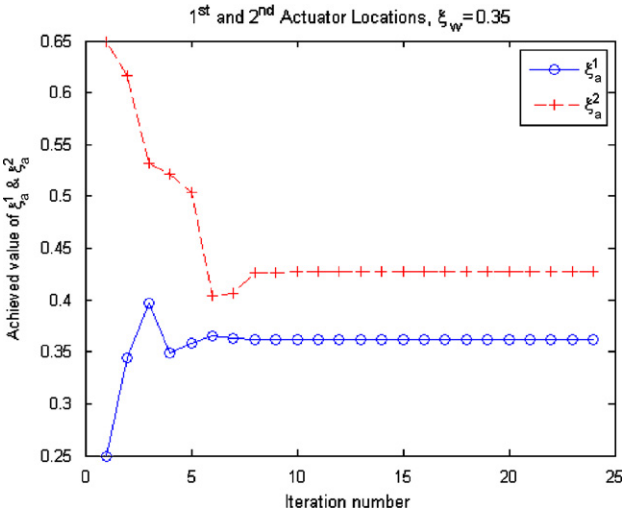

Fig. 9. Iterations and convergence to the optimum locations with the method presented in Ref. [10].

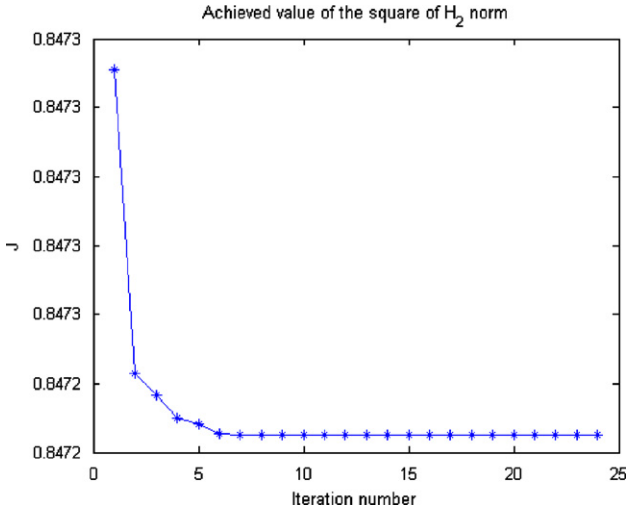

Fig. 10. Iterations and the minimized $\mathscr{H}_2^2$ with the method presented in Ref. [10].

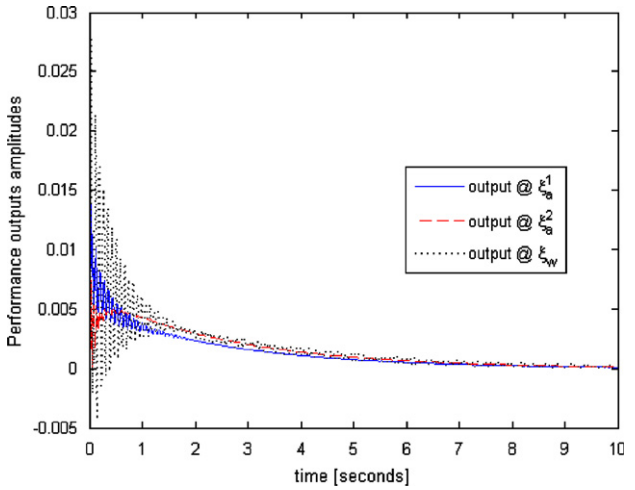

Fig. 11. Impulse response of the beam with actuators at initial locations ($\xi_a^1 = 0.25L, \xi_a^1 = 0.65L$).

high as possible as mentioned in Hiramoto et al. [10]. Fig. 16 shows the variance of the optimal actuator and sensor location with α.

In Figs. 17 and 18, α is kept constant, but the coefficient C_{Ww} of the disturbance input weight is changed. As C_{Ww} increases, the minimized optimization function decreases. That is, as there are less disturbances acting in higher frequencies, the closed-loop $\mathscr{H}_2$-norm decreases at the optimal location of actuator and sensor pair.

5.3. Effect of disturbance weights

To further illustrate the effect of signal weights, the bandpass filter

$$W_{\text{dist}} = \frac{16s^2}{s^4 + 5.657s^3 + 3125s^2 + 8794s + 2.417^6}$$

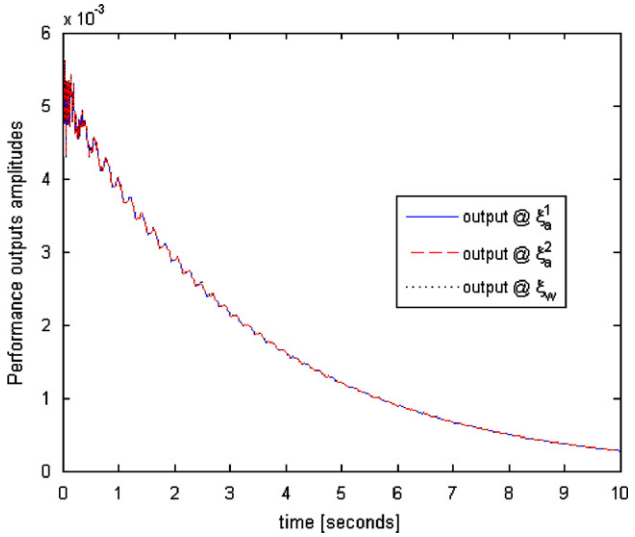

Fig. 12. Impulse response of the beam with actuators at final locations ($\xi_a^1 = 0.35L, \xi_a^1 = 0.35L$).

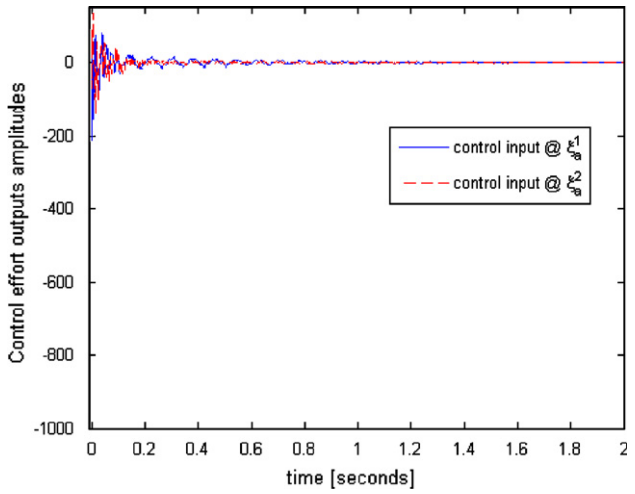

Fig. 13. Control effort impulse response of the beam with actuators at initial locations ($\xi_a^1 = 0.25L, \xi_a^1 = 0.65L$).

is applied as the disturbance input filter. This second-order Butterworth filter is depicted in Fig. 19 and is used to stop all modes other than the second one.

However, if the bandpass filter in Fig. 19 is selected as the disturbance input filter, the optimal locations converges to the points $(0.25L, 0.25L)$, which is one of the antinodes of the second mode of a simply supported beam, as can be seen in Fig. 20.

If the simply supported beam is excited only at its second mode, the maximum deflections occur at points $0.25L$ and $0.75L$ and the point $0.50L$ becomes the node where the deflections vanish. Hence, the optimal locations in the Butterworth filter example seem to reflect this phenomenon correctly and the optimal locations converge to points $0.25L$ or $0.75L$, but not the point $0.35L$, where the disturbance is acting. This result shows that the optimization technique introduced in the study can be can effectively handle the plants shaped with different signal weightings. However, the formulation given in Hiramoto et al. [10] does not consider the signal weightings in the controller design stage.

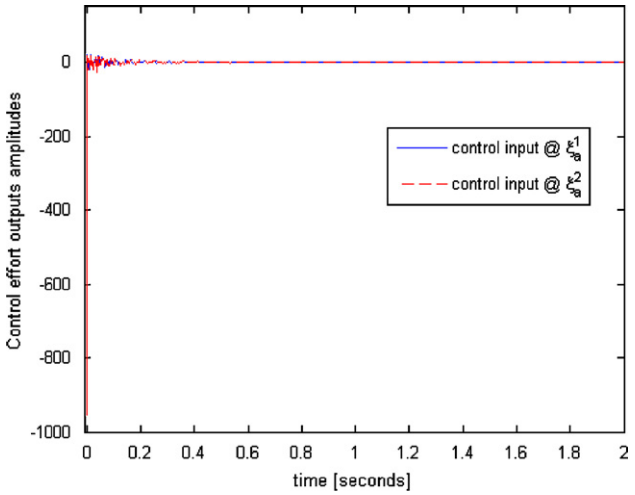

Fig. 14. Control effort impulse response of the beam with actuators at final locations ($\xi_a^1 = 0.35L, \xi_a^1 = 0.35L$).

Table 1
The signal weightings used simulation in Figs. 15–18

	Figs. 15 and 16	Figs. 17 and 18
α	α_c [a]	1
W_{dist}	$\dfrac{10}{0.03s+1}$	$\dfrac{10}{C_{Ww}s+1}$ [b]
W_{in}	$\dfrac{1}{25}$	$\dfrac{1}{25}$
W_{er}	1	1
W_{sn}	$\dfrac{1}{10^5}$	$\dfrac{1}{10^5}$

[a] α_c takes: $1, 2, 3, 4, 5, 10, 20, 20, \ldots, 80, 90, 100$.
[b] C_{Ww} takes: 0, 0.0333, 0.0667, 0.1, 0.1333, 0.1667, 0.2, 0.2333, 0.2667, 0.3.

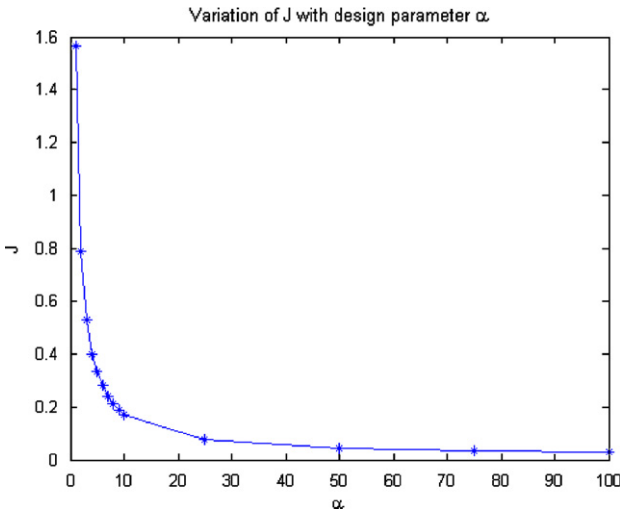

Fig. 15. The minimized $J = \mathscr{H}_2^2$ versus design parameter α.

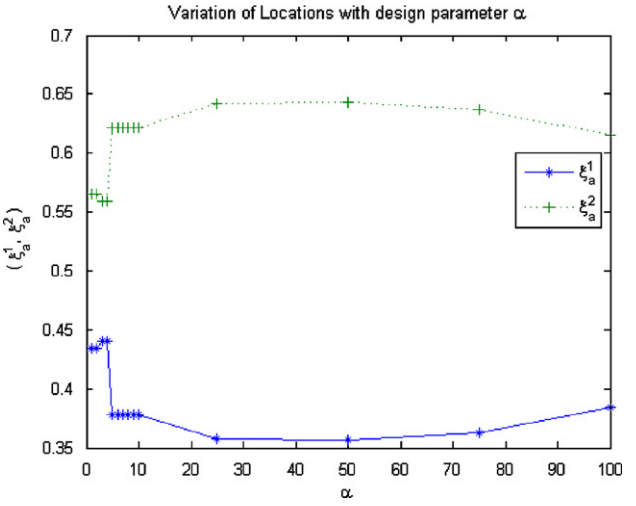

Fig. 16. The actuator/sensor locations versus design parameter α.

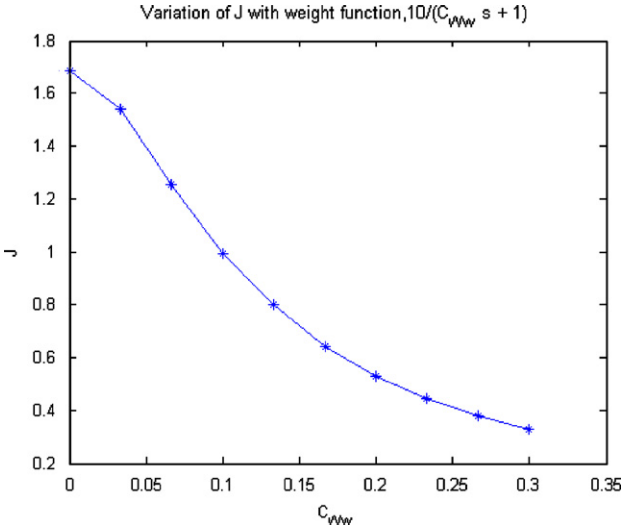

Fig. 17. The minimized $J = \mathscr{H}_2^2$ versus change in disturbance weight coefficient C_{W_w}.

5.4. *The optimal actuator and sensor locations for* $\xi_w = [0.35L, 0.45L]$

One another advantage of our approach is the possibility of using different signal weightings for different channels. This is demonstrated by three cases.

In case 1, both of the disturbances are applied the input signal weighting, $W_{\text{dist}} = 10/0.03s + 1$, in Eq. (42). In this case the optimal locations of the collocated actuator and sensor pair converges to locations where the disturbance input act (Fig. 21).

In case 2, the signal weight for the disturbance input at $\xi_w = 0.35L$ is kept, whereas the bandpass filter in Fig. 19 is used for the disturbance input at $\xi_w = 0.45L$. The obtained optimal locations are to be seen in Fig. 22.

In case 3, the bandpass filter is applied to the disturbance input at $\xi_w = 0.35L$ and the input at $\xi_w = 0.45L$ is filtered with the low-pass filter (see Fig. 23). In this case, both of the optimal locations converge to point 0.45, whereas the optimal locations approach the point $0.35L$ in case 2.

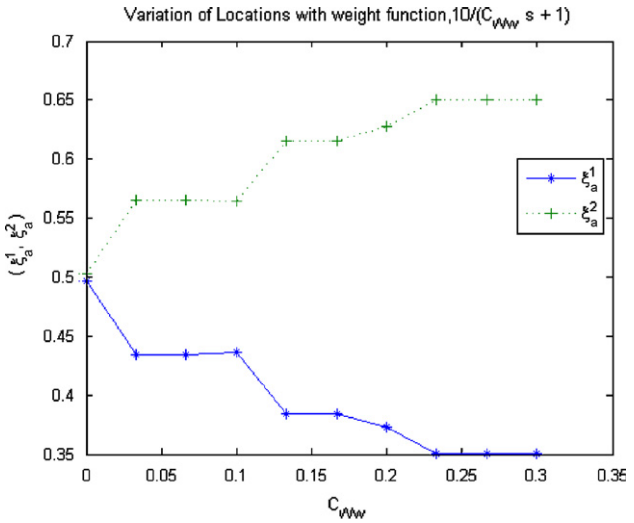

Fig. 18. The actuator/sensor locations versus change in disturbance weight coefficient C_{W_w}.

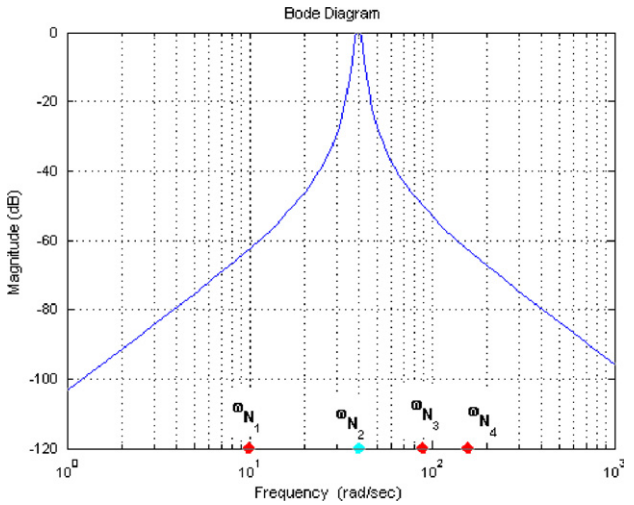

Fig. 19. The disturbance input filter (ω_{N_i} are the natural frequencies of the beam).

In case 4, the bandpass filter is applied to both of the disturbance inputs ($\xi_w = 0.35L, \xi_w = 0.45L$). Similar to the example given in Section 5.3, the optimal locations converge the first antinode of the second mode of the simple supported beam as can be in Fig. 24.

If the disturbances act at different frequencies, the improved coprime controller takes this into account, whereas the controller used by Hiramoto et al. [10] can not.

6. Conclusions and future work

A closed-loop optimal location selection method for actuator and sensor pairs in flexible structures is developed and an example with simple supported beam is given to show the effectiveness of the developed optimization approach.

Using a coordinate transformation, the state matrix of the generalized plant is block diagonalized such that each mode can be dealt individually. This enables the solutions of the generalized AREs to be assumed in the diagonal form. This makes it possible to solve the AREs in the closed form, using quadratic equations.

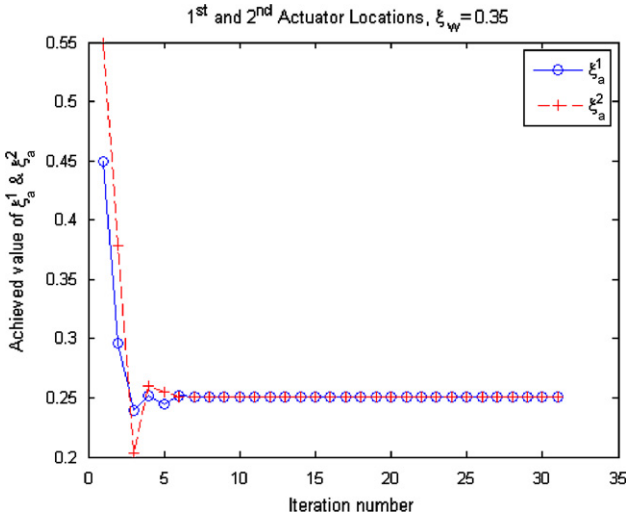

Fig. 20. The actuator/sensor locations with the bandpass filter.

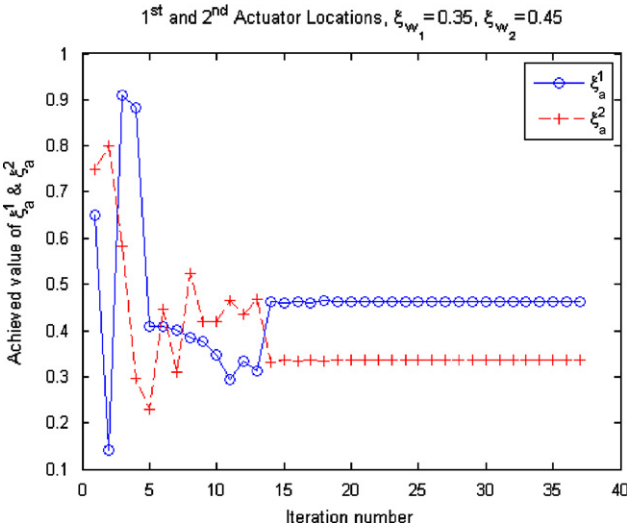

Fig. 21. The actuator/sensor locations (case 1).

Using the concept introduced in Hiramoto et al. [10], a coprime $\mathscr{H}_\infty$ controller is designed. However, modal dampings are not neglected as in Hiramoto et al. [10] an the signal weights are incorporated into ARE solutions. For a gradient-based optimization procedure, partial derivatives of the closed-loop system are derived. The derivatives of the closed-loop system include not only the derivatives of the open-loop system, but also the derivatives of the AREs. Hence, differentiating the AREs the Lyapunov equations are obtained. The approximate solutions of the Lyapunov equations are calculated in the same simple fashion as the AREs. When the necessary derivatives are at hand, the gradient of the optimization metric is obtained and the search for the optimal actuator and sensor locations is found with an unconstrained nonlinear optimization algorithm.

The developed optimization technique has several advantages over the methods in the literature:

- It uses the generalized plant with signal weights.
- The control and filter AREs and their are solved approximately by reducing them to simple quadratic equations. In the iterations of the optimal locations selection procedure, solving these quadratic equations consumes less time compared to solving the AREs fully.

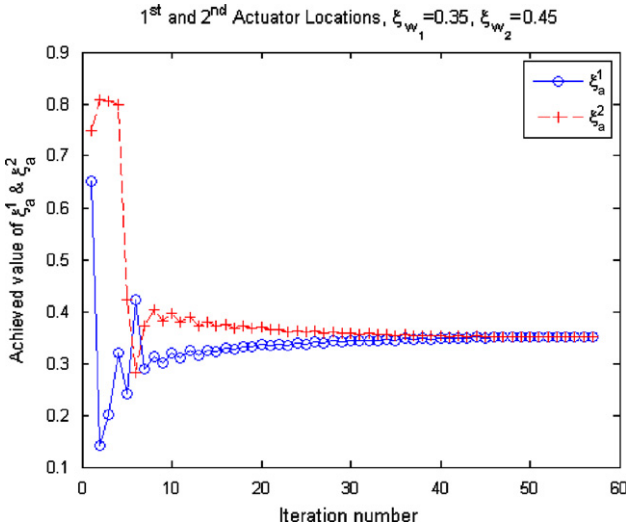

Fig. 22. The actuator/sensor locations (case 2).

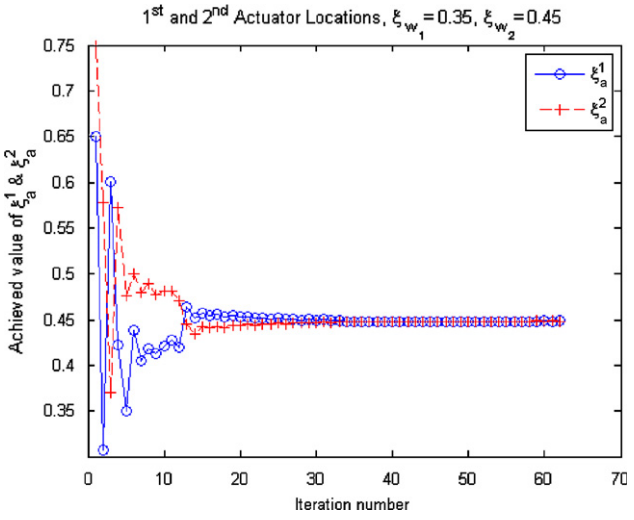

Fig. 23. The actuator/sensor locations (case 3).

- Hiramoto et al. [10] neglect the damping fully, whereas the developed technique uses modal dampings.
- The optimization is done using a closed-loop selection criteria. That is, the objective function is the square of the $\mathscr{H}_2$-norm of the closed-loop generalized plant with the designed controller.
- Closed-loop objectives are incorporated to actuator/sensor location, procedure, through addition of signal weights and forming a generalized plant.

Several additions are possible to our current work. Possible future work includes:

- The best location selection strategy can be applied to smart structures with piezoelectric pathes of arbitrary type of sensors.
- In this study, rate sensors, coupled with first modal form were used so that AREs could be approximately solved. However, using other modal forms one may get also simple solutions of the AREs for displacement sensors.

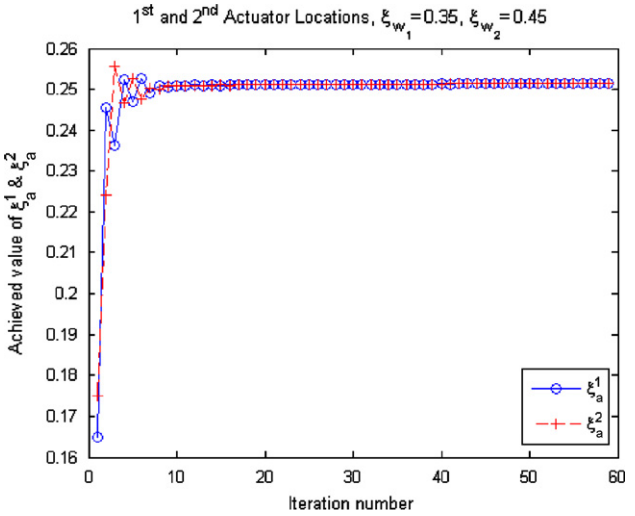

Fig. 24. The actuator/sensor locations (case 4).

- The coprime $\mathscr{H}_\infty$-controller is not obtained for the complete generalized plant P, but for the lower right part of it, P_{yu}. Using the approximate ARE solutions, other types of $\mathscr{H}_2$ and $\mathscr{H}_\infty$ controllers, which use the complete generalized plant, may utilized because they are based on similar AREs.
- The finite element method can be applied to the flexible structures and the optimal actuator/sensor selections technique, which is introduced here, can be applied to discrete models resulting from a finite element analysis with some modifications.

References

[1] M. van de Wal, B. de Jager, A review of methods for input/output selection, *Automatica* 37 (2001) 487–510.
[2] S. Skogestad, I. Postlethwaite, *Multivariable Feedback Control*, Wiley, New York, 1996.
[3] K. Zhou, J.C. Doyle, K. Glover, *Robust and Optimal Control*, Prentice-Hall, Englewood Cliffs, NJ, 1996.
[4] D. Geroges, The use of observability and controllability gramians or functions for optimal sensor and actuator location in finite-dimensional systems, *Proceedings of the 34th IEEE Conference on Decision and Control*, Vol. 4, 1995, pp. 3319–3324.
[5] A. Hać, L. Liu, Sensor and actuator location in motion control of flexible structures, *Journal of Sound and Vibration* 167 (2) (1993) 239–261.
[6] W. Gawronski, K. Lim, Balanced actuator and sensor placement for flexible structures, *International Journal of Control* 65 (1) (1999) 131–145.
[7] P.G. Maghami, S.M. Joshi, Sensor/actuator placement for flexible space structure, *IEEE Transactions on Aerospace and Electronic Systems* 29 (2) (1993) 345–352.
[8] M. Morari, Design of resilient processing plants*iii: a general framework for the assessment of dynamic resilience, *Chemical Engineering Science* 38 (11) (1983) 1881–1891.
[9] A. Arabyan, S. Chemishkian, E. Meroyan, Limits of vibration suppression in flexible structures, *Dynamics and Control* 9 (1999) 223–246.
[10] K. Hiramoto, H. Doki, G. Obinata, Optimal sensor actuator placement for active vibration control using explicit solution of algebraic Riccati equation, *Journal of Sound Vibration* 229 (5) (2000) 1057–1075.
[11] K. Zhou, J.C. Doyle, *Essentials of Robust Control*, Prentice-Hall, Englewood Cliffs, NJ, 1998.
[12] W.K. Gawronski, *Dynamics and Control of Structures: A Model Approach*, Springer, Berlin, 1998.
[13] T. Kailath, *Linear Systems*, Prentice-Hall, Englewood Cliffs, NJ, 1980.
[14] S. Boyd, L. Vandenberghe, *Convex Optimization*, first ed., Cambridge University Press, Cambridge, 2004.
[15] R.T. Haftka, Z. Gürdal, *Elements of Structural Optimization*, Kluwer Academic Publishers, Netherlands, 1992.
[16] U. Kirsch, *Optimum Structural Design*, A McGraw-Hill, Inc., New York, 1981.